Advances in High-Q Piezoelectric Resonator Materials and Devices

Arthur Ballato, *Fellow, IEEE*, and John G. Gualtieri, *Senior Member, IEEE*

***Abstract*—In order to compare piezoelectric materials and devices, an intrinsic parameter, the motional time constant $\tau_1^{(m)} = (\omega_m Q_m)^{-1}$ for a particular mode m is employed. The use of $\tau_1^{(m)}$ follows from the accommodation of acoustic loss in the elastic compliance/stiffness and the establishment of material coefficients that are elements of viscosity matrices. Alternative and fully equivalent definitions of τ_1 are given based on the *RC* time constant derived from the equivalent circuit representation of a crystal resonator, acoustic attenuation, logarithmic decrement, and viscosity or damping. For quartz devices, the variation of τ_1 : for any simple thickness mode, for the $Y'X$ shear mode for rotated Y-cuts, and with diameter-thickness ratio for AT-cuts is discussed. Other factors such as mounting loss and loss caused by crystal inhomogeneities (dislocations, defect positions in the resonator, and impurity migration under vibrational stress) are briefly considered with quartz devices as the model. Some new piezoelectric materials/material constants/devices are reviewed and their motional time constants are compared. A physical parameter, composed of acoustic velocity, piezoelectric coupling, and τ_1 is identified which aids in understanding the maximum frequency limitations of plate resonators.**

I. Introduction

ACOUSTIC-WAVE RESONATORS are used in RF circuits in numerous commercial and military applications. The values of the quality factor, Q, of these resonators (the ratio of the resonant frequency to the full width in frequency at half the maximum amplitude of the conductance [1]) are very high. Thus, these high-Q resonators have great value for use in radio, television, mobile telephone, and high accuracy clocks for time-ordered communications and position-location systems.

In order to compare different piezoelectric materials and devices an intrinsic parameter is employed. We begin with the well-known, experimentally observed relation for high frequency plate resonators of quartz:

$$Q \cdot f = \text{constant}. \tag{1}$$

From this, we invert the product of $Q \cdot \omega$, to obtain a constant parameter having the dimensions of time:

$$\tau_1^{(m)} = (\omega_m Q_m)^{-1}, \tag{2}$$

where $\omega_m = 2\pi f_m$ for a particular resonator mode m. Equation (2) permits calculation of the intrinsic Q of a mode, exclusive of extrinsic factors such as mounting loss and mass loading providing $\tau_1^{(m)}$ is a known constant quantity, presumably related primarily to material parameters. Although derived specifically from quartz resonator data, we shall see below that τ_1 is more generally applicable. This intrinsic parameter τ_1 can alternatively be defined as a motional time constant obtained from the equivalent circuit for piezoelectric resonators, or be defined as a purely physical parameter related to a viscosity tensor of a material, whose matrix elements may be empirically derived from acoustic attenuation and velocity measurements. As such, τ_1 connects electrical engineering and physical descriptions of dissipation in acoustic wave materials and devices.

This paper reviews: i) the concept of motional time constant and its relationship to acoustic loss; ii) losses caused by impurities and their mobility in resonators, by defects and their position in resonators, and by hydrogen nonuniformity in quartz which affects the intrinsic Q; iii) intrinsic properties such as material constants of modern piezoelectric materials of interest for bulk acoustic wave (BAW) and surface acoustic wave (SAW) resonator design; iv) the analysis of real devices in terms of material parameters and resonator geometry using equivalent circuit parameters; v) the frequency/harmonic limits on achieving resonance with plates; and vi) new and advanced resonators in terms of their potential for lowering τ_1.

One objective here is to demonstrate to the user community the value of coordinating and integrating small and perhaps esoteric portions of the large amount of published information available on piezoelectric resonator materials and devices. These seemingly individual and disparate observations form a mosaic, presently incomplete but quite suggestive, of phenomenological acoustic loss mechanisms and their interconnections.

II. Viscosity Definition of τ_1

Lamb and Richter [2], using physical principles involving a viscosity tensor, developed a theory for calculation of the attenuation of acoustic waves in crystalline solids. They used microwave (pulse-echo) measurements to calculate the numerical values of the viscosity matrix for quartz at room temperature. In their theory, small material loss was included by considering the viscosity to be the imaginary part of the elastic stiffness [2]:

$$c^* = c^E + j\omega\eta, \tag{3}$$

where c^E is the stiffness at constant electric field. For specific materials/devices, which are not perfectly lossless, $\tau_1^{(m)}$ is a

Manuscript received November 29, 1993; revised June 7, 1994.

The authors are with the U.S. Army Research Laboratory, Electronics and Power Sources Directorate, AMSRL-EP, Fort Monmouth, NJ 07703-5601 USA.

IEEE Log Number 9405221.

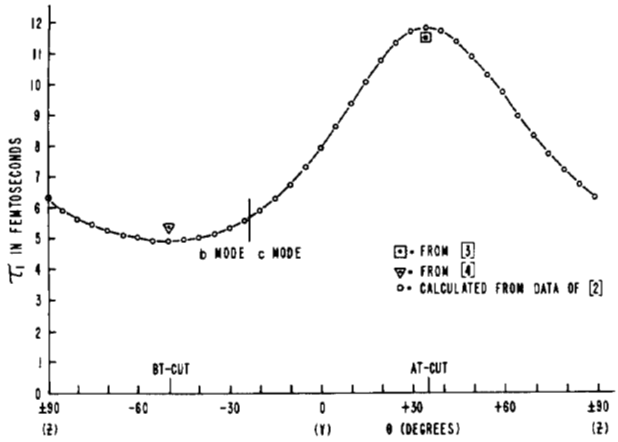

Fig. 1. Time constant, τ_1, for the $Y'X$ shear mode of quartz plates of the orientation $(YX\ell)$ θ calculated from the data of [2].

constant which can alternatively be defined by the equation

$$\tau_1^{(m)} = \eta_m / c_m, \tag{4}$$

where η_m is the viscosity and c_m is the elastic stiffness of the resonance mode, e.g., the high frequency thickness modes of plates. For the pure shear mode in rotated Y-cuts of quartz, τ_1 can be calculated using appropriately transformed viscosity and stiffness values. For this mode, excluding a small piezoelectric contribution, $\tau_1 = \eta'_{66}/c'_{66}$, where

$$c'_{66} = c_{66}\cos^2\theta + c_{44}\sin^2\theta + 2c_{14}\cos\theta\sin\theta \tag{5a}$$

and

$$\eta'_{66} = \eta_{66}\cos^2\theta + \eta_{44}\sin^2\theta + 2\eta_{14}\cos\theta\sin\theta. \tag{5b}$$

Equations (5a) and (5b) suggest that the viscosity and elastic stiffness have the same symmetry. In general, the tensorial symmetries of c and η can be shown to be identical. Besides the stiffnesses, the piezoelectric and dielectric constants are required for a full characterization of acoustic wave propagation in dielectric crystals.

Fig. 1 gives the value of τ_1 for the $Y'X$ shear mode for all rotated Y-cuts as a function of rotation angle θ, using (5a) and (5b) and the data generated by evaluating measurements of the viscosity in quartz published by Lamb and Richter [2]. Data points reported by Bömmel, Mason, and Warner [3] and Seed [4] also are indicated. The graph shows that the BT-cut has nearly the lowest intrinsic loss, about half that of the AT-cut, for a given frequency.

An alternate description of acoustic loss may be described by the use of the fluency tensor in those situations where the elastic compliances are appropriate [5].

III. *RC* Time Constant Definition of τ_1

For a plate resonator of thickness $2h$, and electrode area A, executing simple thickness motion with laterally uniform distribution of motion, the design parameters follow from considering the Butterworth-Van Dyke (BVD) equivalent electrical circuit representation (see Fig. 2) of a crystal resonator in the vicinity of any single resonance. The elements of this

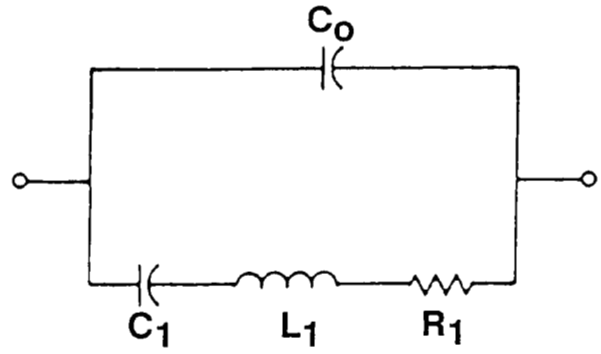

Fig. 2. Butterworth-Van Dyke equivalent circuit. This circuit is an adequate representation of the vibrating crystal in the vicinity of any single resonance.

circuit in terms of material constants and geometrical factors are:

$$C_0 = \epsilon\,(A/2h) \tag{6}$$

$$C_1^{(M)} = 2C_0\,(2k/\pi M)^2 \tag{7}$$

$$R_1^{(M)} = (1/2)\,(\eta/\bar{c})(\pi M/2k)^2(1/C_0) \tag{8}$$

where M = the harmonic for a particular mode m, ϵ is the dielectric permittivity in the thickness direction, and k^2 in (7) and (8) is the square of the piezoelectric coupling coefficient:

$$k^2_{(m)} = e^2_{(m)}/\epsilon\bar{c}_{(m)}, \tag{9}$$

with $e_{(m)}$ the effective piezoelectric stress coefficient. The $\bar{c}_{(m)}$ are the real roots of an eigenvalue equation. They determine, with the mass density ρ, the piezoelectrically stiffened phase velocities

$$v_m = (\bar{c}_{(m)}/\rho)^{1/2}. \tag{10}$$

The static capacitance C_0 arises from the "real" capacitor formed by the electrodes of area A placed on the dielectric of thickness $2h$ and permittivity ϵ. C_1 and R_1, in contrast, are fictional circuit elements arising because of the piezoelectrically driven motion. Each contains the geometrical factor $(A/2h)$ or its inverse [see (6)–(8)], multiplying material factors. We can define two quantities that are functions of material only. These are the motional permittivity $\Gamma_1^{(M)}$ and the motional resistivity $P_1^{(M)}$:

$$\Gamma_1^{(M)} = C_1^{(M)}(2h/A) = \epsilon/r^{(M)} \tag{11}$$

$$P_1^{(M)} = R_1^{(M)}(A/2h) = (1/2)\,\eta\,(\pi M/2e)^2 = \tau_1/\Gamma_1^{(M)} \tag{12}$$

where $r^{(M)} = C_0/C_1^{(M)} = (1/2)\,(\pi M/2k)^2$. In the product

$$P_1^{(M)}\Gamma_1^{(M)} = R_1^{(M)}C_1^{(M)} = \tau_1 = \eta/\bar{c}, \tag{13}$$

the geometrical factors cancel and τ_1, excluding temperature and device-related loss effects, is independent of harmonic and geometry.

Although applied here, for purposes of uncomplicated illustration, to a flat plate resonator executing simple thickness motion, the BVD circuit parameters may be related to ρ, ϵ,

TABLE I
EQUIVALENT DEFINITIONS OF THE TIME CONSTANT τ_1

Definition	τ_1 (seconds)	Remarks
Equivalent Electric Circuit	$R_1C_1=P_1^{(M)}\Gamma_1^{(M)}$	$\tau_1=1/\omega_m Q_1 \propto Q_1^{-1}$ $\omega_m^2 L_1 C_1=1$ $Q_1=(1/R_1)(L_1/C_1)^{1/2}$
Acoustic Attenuation	$2vA/\omega_m^2$	A=attenuation/length (nepers/meter) v=acoustic velocity $=(c/\rho)^{1/2}$
Acoustic Log-Decrement	$\delta/\pi\omega_m$	δ=decrement per period of acoustic wave
Viscosity or Damping	η/c	c=effective elastic constant; η=absolute viscosity in (kg/m-sec) $\rho(\partial^2u/\partial t^2)=c(\partial^2u/\partial x^2)+\eta(\partial^3u/\partial x^2\partial t)$

e, c, η, and geometry in more involved cases as well. The time constant defined here in terms of the product R_1C_1 suggests that it is a resonator parameter. However, it has a more fundamental interpretation in terms of the elastic stiffness and viscosity factors appearing in the elastic wave equation:

$$\rho(\partial^2u/\partial t^2)=c(\partial^2u/\partial x^2)+\eta(\partial^3u/\partial x^2\partial t), \qquad (14)$$

where u is the displacement. Because of this, τ_1 may be equivalently evaluated from the results of attenuation and velocity measurements. Equivalent definitions of τ_1 are given in Table I.

A. Material Constants

Piezoelectric materials for acoustic wave devices have changed markedly over the past twenty years in terms of both the types of materials available and the quality of the individual samples. The total family of acoustic wave materials now used, or under development, includes piezoelectric glass-ceramics having crystallographic and polar orientation and crystals of symmetry classes mm2, 32, 3m, 4mm, 6mm, and $\bar{4}$3m. The symmetry classes 6mm and $\bar{4}$3m also occur frequently in piezoelectric semiconductor materials that are now available in both bulk and thin-film configurations. The various reported values of the material constants of interest for BAW and SAW device applications have been brought together and recently published [6].

The relevant material constants include mass density ρ, elastic stiffness $c_{\lambda\mu}$, piezoelectric stress $e_{i\lambda}$, dielectric permittivity ϵ_{ij}, and thermal expansion coefficients α_{ij}. Viscosity data are, at present, not abundant. Except for the semiconductor materials, only data published after 1978 are included in [6], since the reference literature (Landolt-Börnstein) amply covers those years prior to 1978 [7].

An example of a promising material, under development now, is langasite ($La_3Ga_5SiO_{14}$) [8]–[12]. This material has the same symmetry class as α-quartz (class 32). Large good-quality single crystals are already available [11]. The material constants for langasite are given in Table II, as an illustration of the information available in [6]. These can be used to evaluate τ_1 using the time constant definition. For langasite, using

TABLE II
MEASURED PROPERTIES OF LANGASITE AT ROOM TEMPERATURE

Formula		Symmetry		References	
$La_3Ga_5SiO_{14}$		32		[8-11]	
Property (units)		**[8]**	**[9]**	**[10]**	**[11]**
Density (10^3kg/m^3)	ρ	5.754*		5.743	5.751
Elastic Stiffness (Constant E) (GPa)	c_{11}	190.9	188.9(-58.7)	190.2(-47)	190.2(-47)
	c_{12}	106.3	104.6(-218)	106.3(-100)	106.3(-100)
	c_{13}	104.2	96.8(-101)	91.9(-130)	91.9(-130)
	c_{14}	15.2	14.3(-154)	14.7(-370)	14.7(-370)
	c_{33}	261.9	262.2(-135)	262.1(-94)	
	c_{44}	52.4	53.9(-79.7)	53.82(-30)	53.4(-30)
	c_{66}	43.2	42.2(139)	42.0(+36)	42.35(+36)
Piezo-Electric Stress Constant (C/m^2)	e_{11}	-0.45	-0.44(-2400)		-0.45
	e_{14}	0.077	0.07(-5000)		0.077
Dielectric Constant (ϵ_0)	ϵ^S_{11}	18.87	18.86(447)@		19.0(153)
	ϵ^S_{33}	49.32	49.10(-618)@	~49(-760)+	49.2(-760)
Thermal Expansion	α_{11}		(5.84)	(5.11)	(5.15)
	α_{33}		(4.03)	(3.61)	(3.65)

Note: Numbers in parentheses are temperature coefficients $\times 10^{-6}$/K. *See [12]. @These values are for ϵ^T. +See graph in [10].

published data [8], [9], [13], τ_1 can be calculated for the non-temperature compensated X-cut (pure longitudinal mode along [11$\bar{2}$0]) to be 4.2 fs. A temperature compensated cut (both first- and second-order temperature coefficients $\approx$0 at room temperature) is the Y-cut (pure shear mode along [10$\bar{1}$0]). For this mode, τ_1 is 6.3 fs. The motional time constants were calculated using acoustic attenuation and velocity values reported in [13]. It is expected that acoustic wave devices research on this material will flourish over the next few years; see Section VI-C. in this connection.

In general, the values of material constants are derived from measurements on real crystals and are, therefore, influenced by crystal stoichiometry, purity, and defects. What we have learned from extensive R&D with quartz material will help us to understand acoustic loss in future crystal systems. A short discussion of some of these factors for the case of α-quartz follows.

IV. IMPURITIES

The growth of high purity crystals is a prerequisite for high-Q devices. For AT-cut quartz at room temperature, τ_1 is $\sim$10 fs with corresponding relaxation frequencies ($1/\tau_1$) at $\sim 10^{14}$ Hz or a wavenumber $\approx 3.33\times10^3$ cm^{-1} in the infrared region. This provides an intuitive connection with the use of infrared absorption as a quality control measure for inspection of cultured quartz. The IR absorption can be related to an intrinsic Q or Q_{IR} which is found to be correlated with the mechanical Q of resonators made from the material.

A. Hydrogen in α-Quartz

In the case of hydrothermally grown quartz, it seems clear that hydrogen is the major impurity. Aines *et al.* [14] have found that near the seed, the dominant impurity is molecular

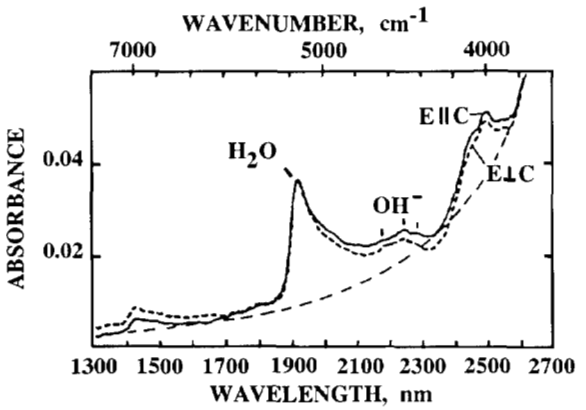

Fig. 3. Near-infrared polarized spectra of a typical quartz sample. Displayed are spectra recorded with E || C (solid line), E ⊥ C (dotted line), and background O-H stretch (dashed line). Beam path was parallel to the seed plate and 3.44 mm from the seed. Sample thickness was 2.44 cm [14].

H_2O. The H_2O concentration decreases away from the seed while OH^- rises in concentration. Typically, the H_2O level remains above the OH^- level up to distances of ~2 cm from the seed. The major species responsible for hydrolytic weakening in quartz appears to be H_2O. The water is present as small groups of H_2O molecules. H_2O is more likely found in rapidly grown quartz. The near-IR spectra of a typical cultured quartz bar is shown in Fig. 3. Shown are absorption features due to ~850 ppm molecular H_2O at 1920 nm, multiple peaks centered at 2250 nm due to X-OH groups (X =Na, Li, etc.), and two bands due to both H_2O and X-OH at 1410 nm and 2500 nm, respectively. These are superimposed upon a strong background absorption due to X-OH stretch at 2900 nm (3400 cm^{-1}) [14].

Sawyer [15] plotted the relationship (shown in Fig. 4) between infrared absorption at 3500 cm^{-1} ($ALPHA_{3500}$)—due to hydrogen content which is related to Q_{IR} of quartz and the mechanical Q of specially contoured and mounted, precision 5 MHz, 5th overtone quartz resonators. His plot also shows there is very little difference in using either Na_2CO_3 or NaOH [16] as the mineralizer in the hydrothermal growth of α-quartz. In general, the concentrations of other impurities seem to follow the concentration of hydrogen in α-quartz. In particular, the X-plus and Z-growth regions contain roughly equal OH-concentrations, whereas the OH-concentration in the X-minus region is about an order of magnitude higher. The X-plus and X-minus regions have similar concentrations of Al, Li, and Na, whereas the Z-growth regions are usually an order of magnitude lower in concentration for these ions [17]. The growth regions are identified subsequently, in Fig. 9.

B. Mobility of Impurities

Impurities can be either interstitial or substitutional. In α-quartz, interstitial impurities are possible because of the existence of large, open, (1–2 Å) c-axis channels in the crystal structure. This allows the interstitial impurities to be very mobile especially under conditions of high temperature and electric field, used for example, in the electrodiffusion process [18], [19]. This process, used generally in the industry to improve the radiation resistance of quartz resonators, also reduces the tendency of quartz to develop etch channels during etch processing of resonator blanks. Trivalent Al and Fe ions can substitute for silicon during crystal growth. These require unipositive charge compensation to balance the single negative charge of a trivalent ion in a quadrivalent site. The compensation is usually satisfied by alkali-metal ions (Li^+, Na^+, etc.) incorporated at interstitial sites during crystal growth. The alkali-metal ions are removed and replaced by hydrogen during the electrodiffusion process. The substitutional impurities are not removed (replaced) by the electrodiffusion process.

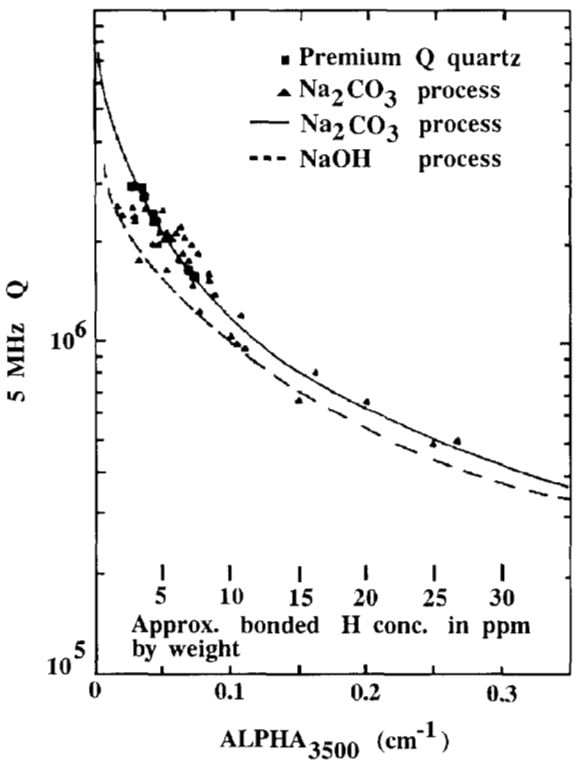

Fig. 4. 5 MHz Q versus $ALPHA_{3500}$ data and empirical curves. Solid curve is plotted from a quadratic in reciprocal Q, computer-fitted to the data shown [15]. Dashed curve was computer-fitted to NaOH "fast grown" quartz data [16].

In the work of Sharp and Pace [20], using quartz resonators, impurity ions have been shown to migrate away from the nodal planes of vibration toward the antinodal planes where the stress of the vibration is a minimum and the stress gradient is a maximum. In Fig. 5 is shown the third harmonic pattern of the strain gradient (ds/dx), strain (s) and the vibrationally induced Raman scattering enhancements (due to the presence of impurity ions which have migrated) versus resonator thickness. The impurity ion in this case was Ag^+ (from the electrodes) whose ionic size and activation energy for electromigration [21] is similar to that of Li^+, a major impurity in α-quartz. By contrast, Cook and Breckenridge [22] indicate that colloidal gold or gold atoms migrate into quartz from electrodes, but appear to migrate to regions of high vibrational stress. Both [20] and [22] report that the migration initially occurred at elevated temperatures (≈250°C). Since these results are not in accordance, the situation is not clear

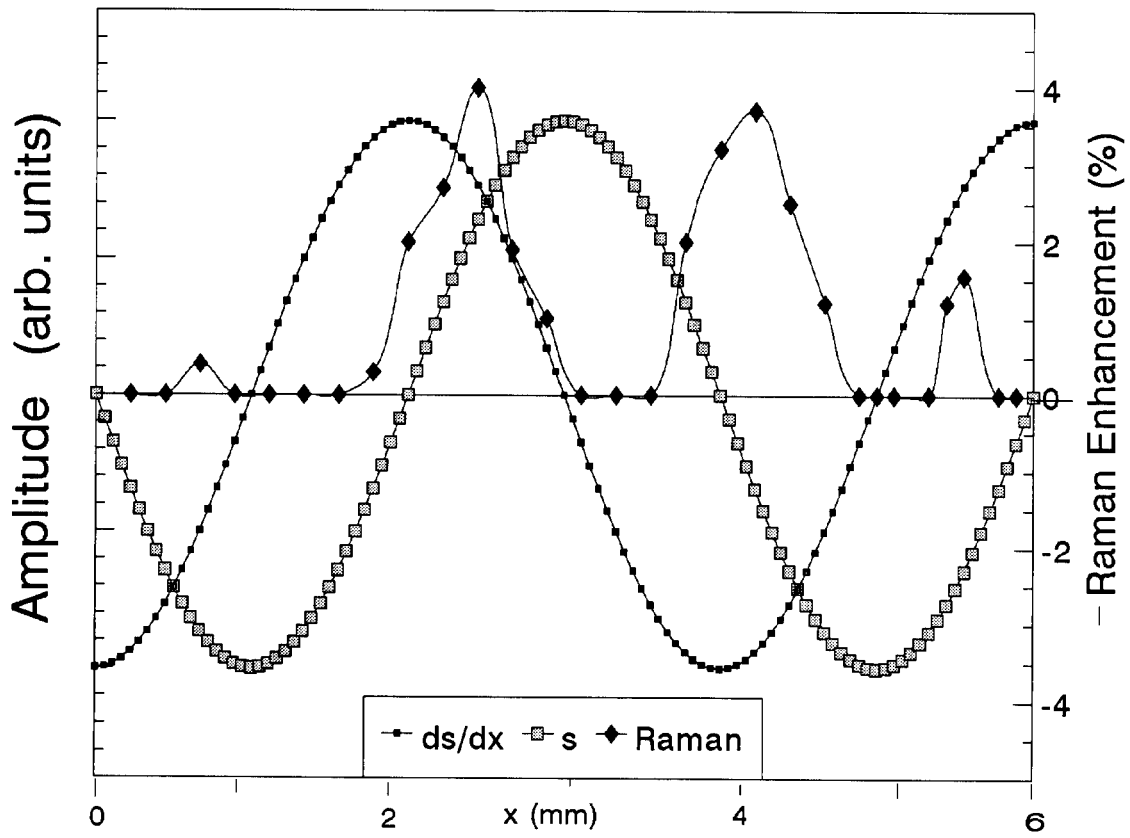

Fig. 5. Third harmonic pattern of strain gradient (ds/dx), strain (s), and vibrationally induced Raman scattering enhancements (due to impurity ions) versus thickness x of a rectangular X-cut prism resonator [20]. The vibrational nodes are located at the zeros of ds/dx.

and further work should be done. In any case, the migration of impurities under vibrational stress increases τ_1 [22].

C. Uniformity of Hydrogen

Uniformity with respect to hydrogen content, which is related to Q, is essential for high device production yields. For lower Q material, quartz bars become less uniform and are subject to easier breakage. However, even high Q material can be subject to nonuniformities. For example, considerable nonuniformity in hydrogen incorporation can result if nonporous electrodes are used in the electrodiffusion process [23], [24]. During nonuniform electrodiffusion, aluminum compensated by electron holes (Al-h^+) develops along with aluminum compensated by hydrogen (Al-OH) [25]. This contributes to nonuniform electrodiffusion along the Z-axis of quartz bars [24], [26], [27] similar to that shown in Fig. 6. In this figure, the integrated absorption of a series of infrared scans taken at various distances along the Z-axis shows considerable nonuniformity in Al-OH and depletion of the as-grown OH band near the anode. These nonuniformities can be largely eliminated if the electrodes used in the electrodiffusion process have a high degree of porosity [24]. Another useful electrodiffusion method is to use electrodes that permit easy diffusion of hydrogen. For example, if electrically conducting amorphous Y-Ba-Cu-O film electrodes, known to allow hydrogen diffusion are used, uniform formation of Al-OH occurs along the Z-axis [24]; see Fig. 7.

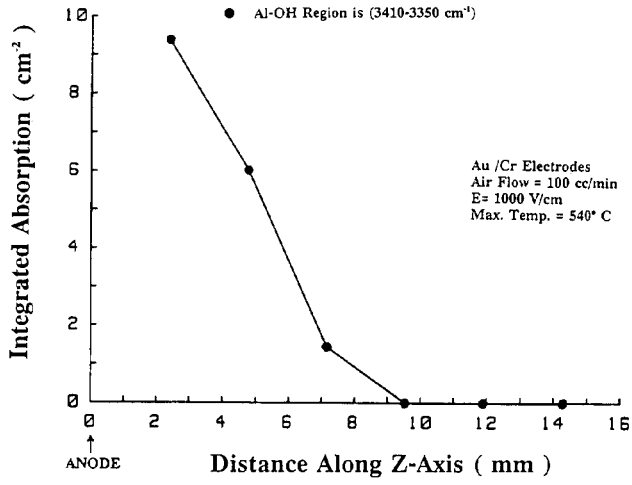

Fig. 6. Integrated infrared absorption (300°K) of a series of spectral scans. The IR beam was unpolarized and in the X-direction. The Al-OH band is nonuniform along the Z-axis [24], [27].

V. Defects

A. Dislocations

Q-values are much affected by the position of structural defects in the resonator. The greatest loss occurs when the defect in a resonator occupies a position close to the nodal plane of the vibration, where the stress of the vibration is the largest [28]. The relation between Q-value and position of a

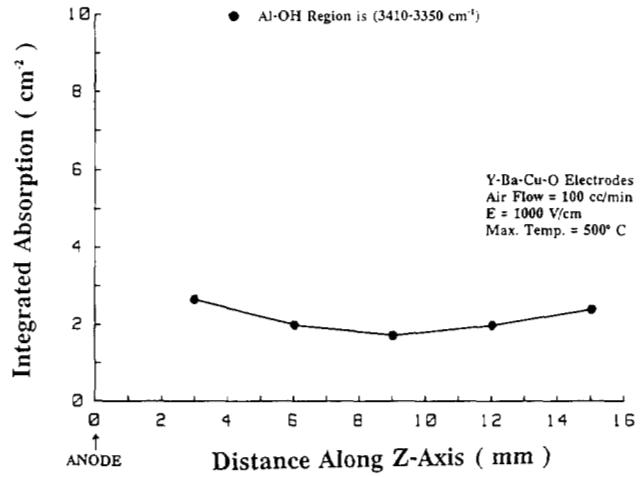

Fig. 7. Integrated infrared absorption (300°K) of a series ofspectral scans (similar to Fig. 6) using Y-Ba-Cu-O electrodes. The Al-OH band is uniform across the bar [24], [27].

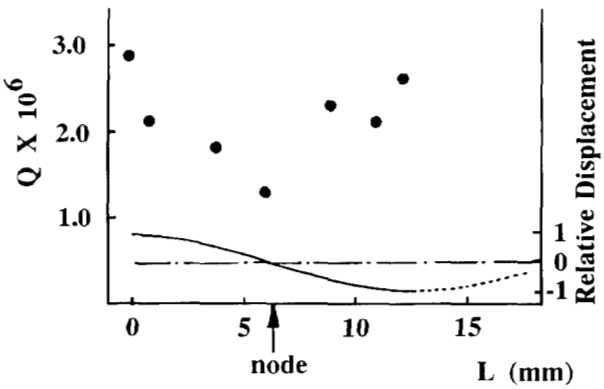

Fig. 8. Relation between Q-values and the position of a defect in a resonator bar. L is the distance from the end of the bar [28].

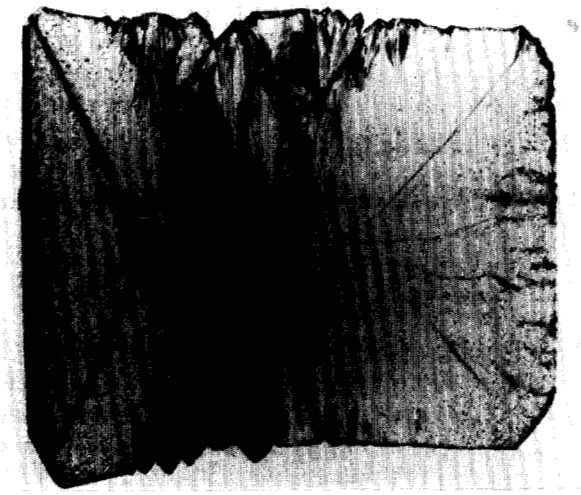

(a)

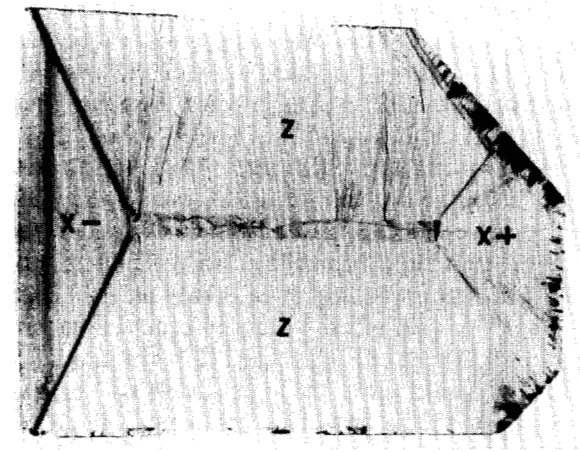

(b)

Fig. 9. X-ray transmission topographs of Y-cross sections of cultured quartz bars grown from Z-seed plates cut from: (a) the Z and (b) X-plus growth regions of previously grown quartz. The growth regions are shown in the X-plus growth sample. *Courtesy of A. Armington, J. Larkin, M. Harris, and J. Horrigan, Rome Laboratory (AFSC) Hanscom AFB, MA 01731-5000.

defect in a resonant bar is shown in Fig. 8. This result suggests that defects in the nodal plane of plate resonators are affected similarly.

Brice [21] reports that there is no unique relationship between dislocation density and hydrogen content. He points out that for any given supplier a linear relationship can be found; however for any given hydrogen content, the dislocation densities for any two suppliers will differ by a factor of 7.4 on average!

The source of dislocations in cultured quartz has been mainly attributed to inclusions, bubbles, the propagation of dislocations present in the seed [29], and lattice parameter mismatch between the seed and the new crystal growth [30]. Some quartz crystal growers [31], [32] have chosen Z-plate seeds from the X-plus growth region to minimize the possibility of dislocations traversing the seed plate (see Fig. 9). Z-seed plates cut from the Z-growth region produce dislocations propagating roughly at right angles to the Z-plate along the direction of the growing crystal. By contrast, Z-seed plates cut from the X-plus growth region produce dislocations propagating at low angles to the Z-face. Thus, the dislocations propagate roughly at right angles to the growth direction. Therefore, fewer dislocations are expected in the new crystal. However, this approach does not address the problem of lattice parameter mismatch and inclusion-caused dislocations. Successful methods to handle these problems have yet to be fully developed.

These extended defects, in both natural and cultured quartz have been studied by many investigators. X-ray topography and etching can be used to show that dislocations are the source of etch channels [33]–[36]. Nielson and Foster [37] have suggested that etch channels were formed by leaching of impurities that had precipitated along dislocation lines. Others have suggested that channel dissolution is aided by the release of potential energy, stored as stress along the dislocation line [38]. Diffraction contrast due to dislocations is revealed in X-ray topographs. The contrast results from the strain field around the dislocation. Comparison of X-ray topographs made on quartz resonator blanks before and after electrodiffusion show very little change in either the diffraction contrast or the number of dislocations [39]. This would indicate that the formation of etch channels is not influenced greatly by the dislocation strain energy. The impurity modification sugges-

tion is more likely for the following reasons: electrodiffusion removes alkali-metal ions and quartz is attacked by alkaline solutions, such as NaOH and Na_2SiO_3 [40]; and reductions in etch-channel density have been found when dislocations were decorated with electrode-metal impurities [41],[42]. Others report that it appears Ca^{++} and Mg^{++} are localized at the distorted lattice surrounding a dislocation and are preferentially removed during etch-channel formation [43].

VI. Resonant Devices

When plane acoustic waves propagate in isotropic substances such as glass, it is found that two types of wave motion are possible. One type is called a longitudinal or compressional wave where the particle motion is parallel to the direction of wave propagation. The other wave, called a shear wave, has motions that are perpendicular to the propagation direction. In fact, there are two shear waves with different polarizations, but identical speeds making a total of three bulk acoustic waves.

When the plane acoustic wave propagates in a crystal such as quartz, it is found that there are still three waves, but each contains both shear and longitudinal motions. These are called quasi-longitudinal and quasi-shear waves, depending upon which motion is predominant. When verbal precision is not an issue, the qualifier "quasi" is usually dropped. The two shear waves in general have different speeds; they are both slower than the compressional wave. The three particle motions associated with the three waves are still mutually perpendicular to each other, but are in general neither along nor perpendicular to the direction of wave travel. When a crystal is piezoelectric, the propagation of the acoustic wave produces, in the quasistatic approximation, an electric field in the direction of travel. This property affects the generation of acoustic modes in a crystal resonator that uses external electrodes disposed on the major plate surfaces. The presence of piezoelectricity also further tilts the particle motion vectors for the three plane waves, but they remain mutually orthogonal.

If the plane wave (longitudinal or shear) in a piezoelectric medium encounters a free surface parallel to itself, then it will freely reflect as a wave of the same type under certain conditions; in general, the reflection consists of an admixture of all three wave types, depending on the electrical boundary conditions. If there are two such parallel boundaries, the piezoelectric crystal is then called a plate and acoustic waves reflecting back and forth between the free surfaces combine to constitute modes of vibration at particular frequencies called resonances. If the surfaces are coated with electrodes, then the imposition of electrical boundary conditions in the form of a short circuit, an open circuit, or an impedance condition allows one to adjust the critical frequencies of the vibrating structure. This mechanically vibrating structure can be characterized by the Butterworth-Van Dyke equivalent circuit in the vicinity of any single resonance.

A. Intrinsic Properties and Device Geometry

It is important to understand the limitations resulting from the material itself and the limitations resulting from the geometry of the device in a particular application. The intrinsic internal friction in quartz, for example, limits the maximum obtainable Q. The room temperature intrinsic Q of 16×10^6 at 1 MHz can be found from the well-known curve of Warner [3] shown in Fig. 10. Intrinsic Q and frequency are inversely related such that $Q \cdot f$ is constant. The data in Fig. 10 were obtained by evaluating quartz plates of different frequencies, sizes, and configurations. All groups of resonators have peaks of their Q-values which occur at different frequencies. The peaks are, approximately, the intersections on a log-log scale of two straight lines with slopes of $+1$ and -1. The -1 slope is fixed by the f^{-1} dependency of Q. It represents a limitation imposed by the quartz itself. The $+1$ slope is an indication that "mounting" losses become increasingly greater when a quartz plate of a given diameter is operated at decreasingly lower frequencies. Based on the data of Fig. 10, the average τ_1 values are plotted in Fig. 11 versus the dimensionless parameter, the diameter-to-thickness ratio. In comparing Fig. 10 to Fig. 11, the separate curves of Fig. 10 for various values of diameter are normalized and grouped closer together in Fig. 11. Lines of positive unit slope in Fig. 10 become lines of -2 slope, while those of negative unit slope become lines of zero slope in Fig. 11. The zero slope region indicates the presence of a constant intrinsic loss, independent of plate geometry. The intrinsic value of τ_1 for AT-cut resonators is $\sim$10 fs. Fig. 11 shows that this value is closely approached in some cases. In other cases, the presence of other loss mechanisms such as mounting losses and acoustic energy lost to unwanted modes result in higher values of effective τ_1.

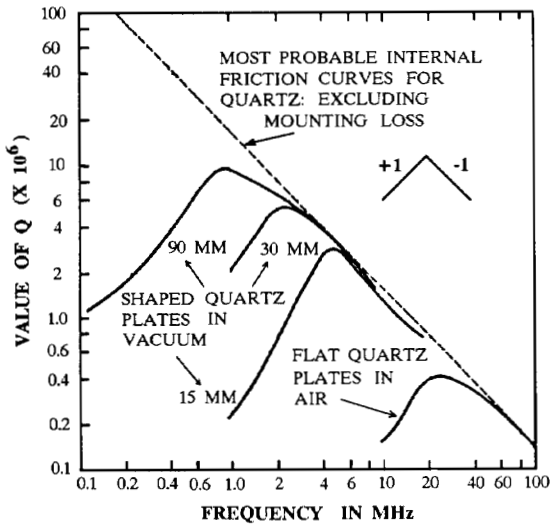

Fig. 10. Values of Q for AT-cut shear vibrating plates of different frequency, size and configuration, and the most probable Q versus frequency for quartz itself [3]. Slopes of -1 and $+1$ are depicted.

The plane wave concept assumes the plate has infinite lateral extension. If a real resonator plate has a diameter 50 to 100 times its thickness, then the plate appears infinite in comparison to the propagating acoustic wavelength. In this case, lateral variations in the wave do not have to be considered. When these lateral variations can be neglected, the modes are called simple thickness modes. For bulk wave resonators with large diameter-to-thickness ratio, it is easy

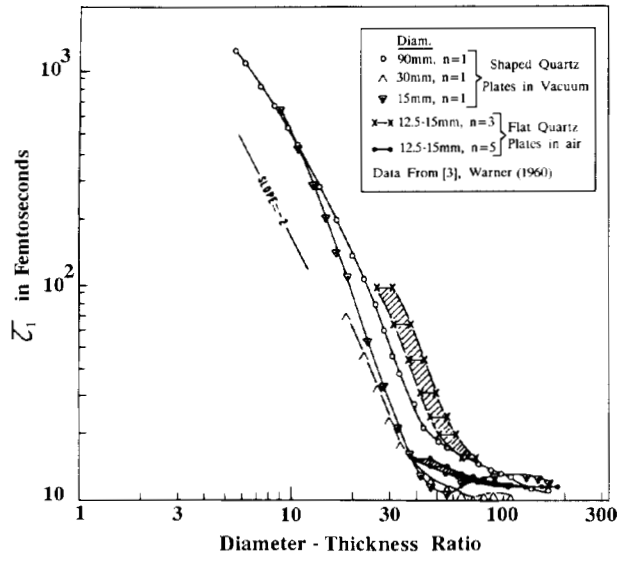

Fig. 11. Time constant τ_1 for AT-cut quartz plates as a function of diameter-thickness ratio, average values. Plate diameters and overtones (n) are given in the legend [46].

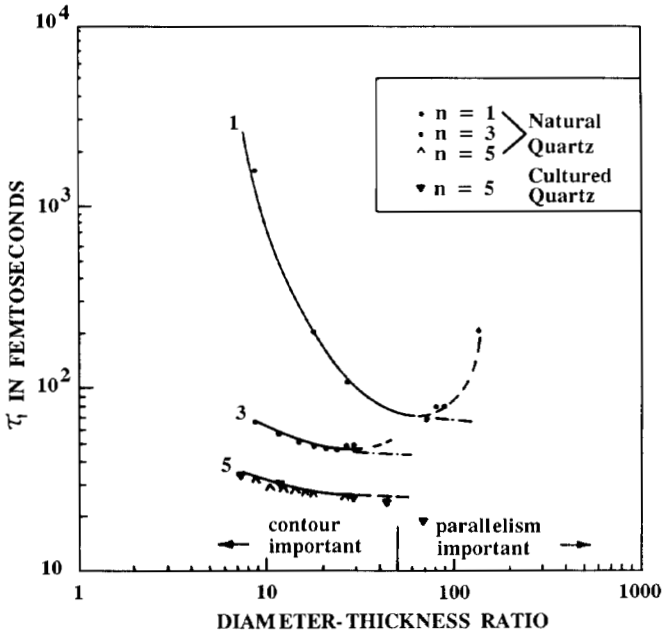

Fig. 12. Time constant τ_1 for shaped, AT-cut, quartz plates in air as a function of diameter-thickness ratio, with overtone (n) as parameter, minimum values, room temperature [46].

to design the mounting structure such that only the intrinsic friction in the material is involved in the time constant. As the diameter-to-thickness ratio becomes much lower than 50, mounting losses increase and must be considered. The general case of simple thickness modes, too comprehensive to be discussed here, is treated in [44] and for the same reason, the practical aspects of quartz resonator design are adequately addressed in [45], including how the effective time constant, τ_1, increases with diameter-to-thickness ratio. Fig. 12 shows that a diameter-to-thickness ratio of about 50 represents a dividing line. For ratios below 50, contouring and mounting are important. For ratios greater than 50 the τ_1 should be constant, but the figure shows τ_1 increases in some cases. This is attributed to lack of parallelism of the crystal blank faces. For large ratios, maintaining sufficient parallelism becomes important [46].

B. Limits on Achieving Resonance with Plates

What are the maximum frequency/overtone limits imposed on plate resonators by material values? The following argument is an attempt to answer this question.

The figure of merit, $\mathcal{F}$ of a resonator is defined as [1], [45], [47]

$$\mathcal{F} = Q/r. \tag{15}$$

In [47] it is justified that when a resonator ceases to possess an inductive region, i.e., when the resonant and antiresonant frequencies are equal ($f_R = f_A$), resonance ceases and at this point it is explained in [45], [47] that $\mathcal{F} \approx 2$. If we want to relate maximum operating frequency and maximum useable harmonic for a material we set $\mathcal{F} = 2$; then

$$\begin{aligned}\mathcal{F} = 2 = Q/r &= (2\pi\tau_1)^{-1}(1/f)\,(8k^2/\pi^2)\,(1/M^2) \\ &= (4k^2/\pi^3\tau_1)\,(fM^2)^{-1},\end{aligned} \tag{16}$$

so

$$fM^2 = 2k^2/\pi^3\tau_1 = \text{constant}. \tag{17}$$

This gives the maximum operating frequency for a given overtone (and material). Further, if we can relate frequency to harmonic and thickness ($t = 2h$):

$$\begin{aligned}f^{(M)} &= f = \text{operating frequency at the } M\text{th harmonic.} \\ &= N_0 \cdot M/t,\end{aligned} \tag{18}$$

where N_0 = "frequency constant" = $v/2$ and v is given in (10). Thus,

$$f^{(M)} = f = N_0 \cdot M/t. \tag{19}$$

If we introduce this into (17) we obtain:

$$M^3 = (2k^2/\pi^3\tau_1 N_0) \cdot t = (\text{constant}) \cdot t, \tag{20}$$

where M is the maximum harmonic that can be used at the resonator thickness t and still have a point of zero reactance ($f_R = f_A$, or $\mathcal{F} = 2$). Since $(2k^2/\pi^3\tau_1 N_0)$ has dimensions of [meter^{-1}], we can choose to call it the reciprocal of a characteristic length = L_0^{-1}. L_0 has this meaning: it is the thickness ($t = 2h$) for which the maximum useable overtone is unity (fundamental harmonic). Thus:

$$M_{\max}^3 = (t/L_0). \tag{21}$$

For AT-cut quartz, $k^2 \approx 0.77\%$, $\tau_1 \approx 11.8$ fs, $N_0 \approx 1661$ m/s and, therefore, $L_0 \approx 39$ nm or 390 Å. The operating frequency at $M_{\max}$ is, using (18) and (21),

$$f = N_0(L_0 t^2)^{-1/3}. \tag{22}$$

If we define $f_0 = N_0/L_0$ as the fundamental frequency of a plate of thickness L_0, and $f_1 = N_0/t$ as the fundamental frequency of a plate of thickness t, then the operating frequency, f, at maximum useable overtone $M_{\max}$, is

$$f = f_0^{1/3} \cdot f_1^{2/3} = (f_0 \cdot f_1^2)^{1/3}, \tag{23}$$

or f is the geometric mean of f_0 and f_1^2.

The characteristic length, L_0, is a critical physical parameter that incorporates acoustic velocity, piezoelectric coupling, and phonon viscosity. Listed in Table III are motional time constants and characteristic lengths for advanced piezoelectric materials/cuts of interest. Using (21) and (22) the relationships between frequency, harmonic and thickness are plotted in Fig. 13 for a few of these materials/cuts. Besides viscosity, there are, of course, other losses to be considered, such as ambient, mounting, electrode films—especially for very thin membranes, and contact resistance. However, for plate resonator operation, the minimum thickness L_0, is the dominant factor. Thus, the difficult problem in achieving the maximum frequency/overtone limits of plate resonators is not the Q of the device but the fabrication of very thin and uniform membranes with thin and low resistance electrodes. Equation (22) is plotted in Figs. 13(a) and (b) for the materials/cuts of interest. Also plotted on each curve are the discrete harmonic points from (21). One sees the future potential for these resonators for direct operation at radar frequencies.

C. Recent Advances

A number of advances using new resonator designs have recently been reported. These include bulk resonators employing surface transverse wave (STW) structures [48], mini-BVA [49], and new crystal cuts using quartz [50] and dilithium tetraborate [51]. Advanced resonator devices using thin-film technology should be included with this group. Most thin-film research has been concentrated on composite resonators employing ZnO and AlN piezoelectric films on substrates of GaAs or Si [52]. Use of these substrates does not allow motional time constants below ~16 fs. Reductions in this motional time constant will require the use of low acoustic loss substrates such as sapphire. Edge-supported ZnO and AlN thin-film resonators have been reported, but these have time constants above 30 fs [52]. Lower τ_1 edge-supported devices are possible if higher quality piezoelectric materials can be fabricated in thin-film form. In addition, low τ_1 devices can be realized with overmoded resonators using piezoelectric films as transducers to excite waves in low acoustic loss substrates having parallel surfaces [53]. If the substrate is many acoustic wavelengths thick, the resonator operates at a large mode number and at a low τ_1. (See Table III; Fig. 14 gives schematics of the thin-film resonators.)

VII. Conclusion

The motional time constant, τ_1, was employed to compare different piezoelectric materials and devices. Use of the time constant allows interpreting the causes of losses in vibrating devices and assists in attributing the losses to different mechanisms, e.g., intrinsic loss, mounting loss, etc. Because of its fundamental interpretation, τ_1 can be equivalently evaluated using pulse-echo and velocity measurements or by using equivalent circuit parameters.

The equivalent circuit parameters can be evaluated using material constants; however, the measurable material properties are subject to variation depending on impurities (e.g., hydrogen in quartz) and defects. In the example of quartz, all impurity concentrations rise with hydrogen concentration, and high dislocation density directly degrades device performance and also promotes hydrogen incorporation. Also, uniformity with respect to hydrogen content relates to τ_1 and this uniformity is greatly influenced by electrodiffusion processing.

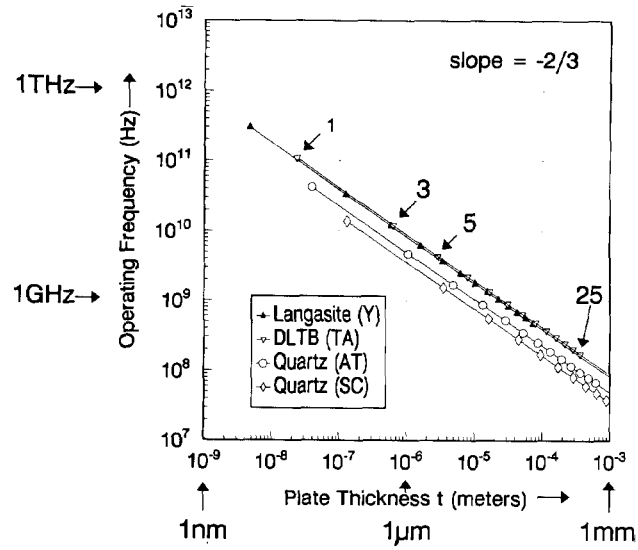

(a)

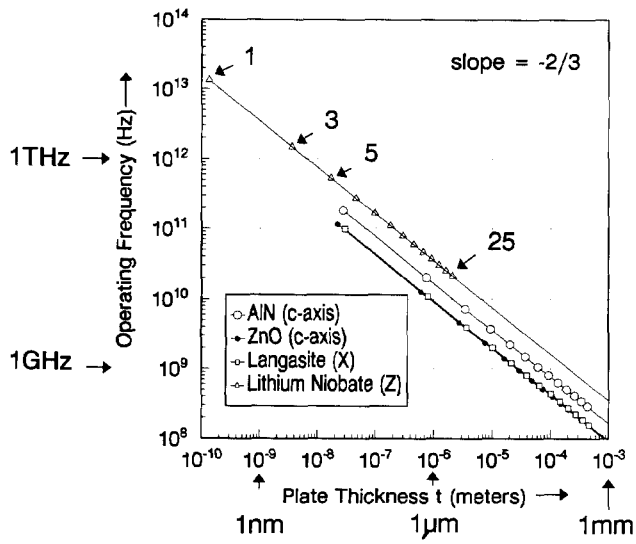

(b)

Fig. 13. Operating frequency versus plate thickness for thin membrane resonators of (a) temperature compensated materials/cuts including: quartz (AT-cut) and (SC-cut), langasite (Y-cut), and dilithium tetraborate (DLTB) (TA-cut), subject to the constraint that the figure of merit $\mathcal{F} = 2$. Symbols indicate harmonics $1, 3, 5 \ldots 25$ at which different resonators of varying thickness operate with this constraint; (b) Same as (a) for nontemperature compensated materials/cuts including: lithium niobate (Z-cut), langasite (X-cut), and aluminum nitride and zinc oxide thin-film edge-supported resonators (c-axis orientation).

TABLE III
MOTIONAL TIME CONSTANTS AND CHARACTERISTIC LENGTHS FOR SOME PIEZOELECTRIC RESONATORS

Type/Cut	N_o (m/s)	Q (X 10^3)	τ_1 (fs)	k^2 (%)	L_o (nm)	Reference
Bulk Resonators						
Quartz (AT)	1,661		11.8	0.77	39.24	[45]
Quartz (BT)	2,536		4.9	0.32	60.99	[45]
Quartz (SC)	1,797		11.7	0.25	130.9	[45]
Quartz (STW)		3.3	24			[48]
Quartz (mini-BVA)		2500	13			[49]
Quartz (TC)		1600	10			[50]
$LiNbO_3$ (Z)	1,787		2.94	60.7	0.13	[58]
$La_3Ga_5SiO_{14}$ (Y)	1,384		6.3	2.89	4.68	[8,9,13]
$La_3Ga_5SiO_{14}$ (X)+	2,892		4.2	0.64	29.42	[8,9,13]
$Li_2B_4O_7$ (TA)*	2,550	450	7.8	1.32	23.36	[51,54]
Thin-Film Resonators						
ZnO (c-axis) (edge-spt'd)	2,500#	7	45	8	21.79	[52]
AlN (c-axis) (edge-spt'd)	5,000#	5	32	9	27.55	[52]

+Measured for the a-mode.

*Measured for the b-mode.

Assuming a thickness of 5 μm.

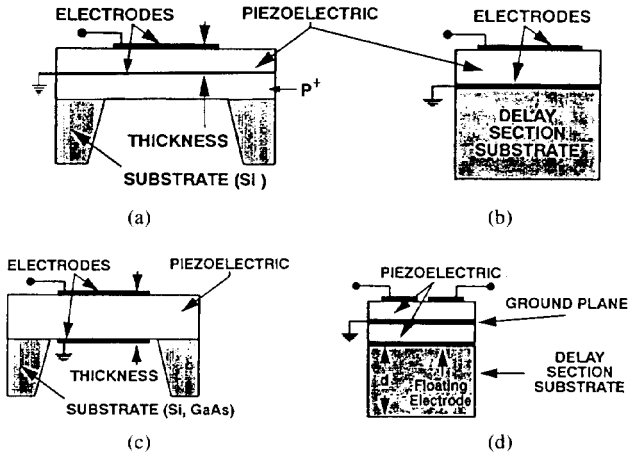

Fig. 14. One- and two-port thin-film resonator configurations for microwave frequencies: (a) a composite structure that uses a p^+ layer as an etch stop for a selective chemical etch, the resultant p^+membrane is used as a platform for subsequent deposition of piezoelectric layers; (b) an overmoded resonator consisting of a thin-film piezoelectric transducer fabricated on a low-loss (Z-cut sapphire) substrate having reflecting surfaces; (c) a thin-film fundamental mode resonator supported by the edges of a substrate; and (d) a stacked crystal filter having two single layers of piezoelectric film, connected in series to bring the output electrode to the surface [53].

In addition, τ_1 can be increased by the mobility of impurities under vibrational stress and the position of defects with respect to high stress regions (nodes) in resonators.

For quartz resonator devices operating above 10 MHz, internal friction losses dominate τ_1. A large part of these losses arises from defects and impurities in the crystal; these are dependent on the growth and postgrowth (electrodiffusion) processes. Since the internal friction has been correlated with IR absorption, a simple IR test can be used for quality control.

For the singular topic of the maximum frequency limit imposed on a resonator plate by material values, a physical parameter L_0, a characteristic length, was identified. This length is the thickness of a plate resonator for which the maximum useable overtone is the fundamental harmonic; it points to the future availability of membrane resonators operating at frequencies well above current limits [45], [55]–[57]. A number of advances leading to low motional time constants by using new materials and new devices were discussed and their characteristic lengths were compared.

ACKNOWLEDGMENT

The authors would like to thank Dr. J. Kosinski for helpful discussions with regard to the langasite material.

REFERENCES

[1] A. Ballato, "Resonance in piezoelectric vibrators," *Proc. IEEE*, vol. 58, no. 1, pp. 149–151, Jan. 1970.
[2] J. Lamb and J. Richter, "Anisotropic acoustic attenuation with new measurements for quartz at room temperature," *Proc. Roy. Soc.*, London, vol. 293A, pp. 479–492, 1966.
[3] H. E. Bömmel, W. P. Mason, and A. W. Warner, "Experimental evidence for dislocations in crystalline quartz," *Phys. Rev.*, vol. 99, pp. 1894–1896, 1955; and A. W. Warner, "Design and performance of ultraprecise 2.5-mc quartz crystal units," *Bell Sys. Tech. J.*, vol. 39, pp. 1193–1217, Sept. 1960.
[4] A. Seed, "The internal friction of synthetic quartz as a function of strain amplitude and frequency," *Brit. J. Appl. Phys.*, vol. 16, pp. 87–91, 1965.
[5] A. Ballato, "The fluency matrix of quartz," *IEEE Trans. Son. Ultrason.*, vol. SU-25, no. 2, pp. 107–108, Mar. 1978.
[6] J. G. Gualtieri, J. A. Kosinski, and A. Ballato, "Piezoelectric materials for acoustic wave devices," *IEEE Trans. Ultrason. Ferroelect. Freq. Contr.*, vol. 41, pp. 53–59, Jan. 1994.
[7] Landolt-Börnstein, *Numerical Data and Functional Relationships in Science and Technology*. Berlin, Heidelberg, New York: Springer-Verlag, 1966, vol. III/1; 1969, vol. III/2; and 1979, vol. III/11.
[8] A. A. Kaminskii, I. M. Silvestrova, S. E. Sarkisov, and G. A. Denisenko, "Investigation of trigonal $(La_{1-x}Nd_x)$ Ga_5SiO_{14}, (II spectral laser and electromechanical properties)," *Physica Status Solidi*, vol. 80, pp. 607–620, 1983.
[9] A. B. Ilyaev, B. S. Umarov, L. A. Shabanova, and M. F. Dubovik, "Temperature dependence of electromechanical properties of LGS crystals," *Physica Status Solidi A*, vol. 98, pp. K109–K114, Dec. 1986.
[10] I. M. Silvestrova, Yu. V. Pisarevskii, P. A. Senyushchenkov, and A. I. Krupnyi, "Temperature dependence of the properties of $La_3Ga_5SiO_{14}$ single crystals," *Soviet Phys. -Solid State*, vol. 28, pp. 1613–1614, Sept. 1986.
[11] S. A. Sakharov, I. M. Larionov, and A. V. Medvedev, "Application of langasite crystals in monolithic filters operating in shear modes," *Proc. 1992 IEEE Freq. Contr. Symp.*, pp. 713–723, May 1992.
[12] A. A. Kaminskii, B. V. Mill, and I. M. Silvestrova, "The nonlinear active material $(La_{1-x}Nd_x)Ga_5$ SiO_{14}," *Bull. Academy of Sci. USSR. Physical Series*, vol. 47, pp. 25–31, 1983.
[13] I. M. Silvestrova, Yu. V. Pisarevskii, B. V. Mill, and A. A. Kaminskii, "Acoustical and electromechanical properties of piezoelectric crystals with a trigonal Ca-gallogermanate structure," *Sov. Phys. Dokl.*, vol. 30, no. 5, pp. 402–403, May 1985.
[14] R. D. Aines, S. H. Kirby, and G. R. Rossman, "Hydrogen speciation in synthetic quartz," *Phys. Chem. Minerals*, vol. 11, pp. 204–212, 1984.
[15] B. Sawyer, "Q capability indications from infrared absorption measurements for Na_2CO_3 process cultured quartz," *IEEE Trans. Son. Ultrason.*, vol. 19, pp. 41–44, 1972.
[16] D. B. Fraser, D. M. Dodd, D. W. Rudd, and W. J. Carroll, "Using infrared to find the mechanical Q of α-quartz," *Frequency*, vol. 4, no. 1, pp. 18–21, 1966.
[17] F. Iwasaki and H. Iwasaki, "Impurity species in synthetic and Brazilian natural quartz," *Japan. J. Appl. Phys.*, vol. 32, pp. 893–901, Feb. 1993.
[18] J. J. Martin, "Electrodiffusion (sweeping) of ions in quartz—a review," *IEEE Trans. Ultrason., Ferroelect., Freq. Contr.*, vol. 35, pp. 288–296, May 1988.
[19] J. G. Gualtieri, "Sweeping quartz crystals," *IEEE Ultrason. Symp. Proc.*, vol. I, pp. 381–391, 1989.
[20] R. R. Sharp and E. L. Pace, "Direct observation of impurity motion effect in quartz using the Raman effect," *J. Phys. Chem. Solids*, Pergamon Press, vol. 31, pp. 2275–2279, 1970.

[21] J. C. Brice, "Crystals for quartz resonators," *Revs. of Modern Phys.*, vol. 57, pp. 105–146, 1985.
[22] R. C. Cook and R. G. Breckenridge, "Anelasticity of quartz," *Phys. Rev.*, vol. 92, pp. 1419–1423, 1953.
[23] J. G. Gualtieri, L. Calderon, and R. T. Lareau, "Update on possible electrode mechanisms in the sweeping of alpha quartz," *Proc. 43rd Ann. Freq. Contr. Symp.*, pp. 509–516, 1989.
[24] J. G. Gualtieri and J. A. Kosinski, "Electrode-induced nonuniformities in the sweeping of alpha quartz," *IEEE Trans. Ultrason. Ferroelect. Freq. Contr.*, vol. 38, pp. 486–493, 1991.
[25] G. B. Krefft, "Effects of high-temperature electrolysis on the coloration characteristics and OH-absorption bands in alpha quartz," *Radiation Effects*, vol. 26, pp. 249–259, 1975.
[26] H. G. Lipson, A. Kahan, and J. O'Connor, "Aluminum and hydroxide defect centers in vacuum swept quartz," *Proc. 37th. Ann. Freq. Contr. Symp.*, pp. 169–176, 1983.
[27] J. G. Gualtieri, "Possible mechanisms for the introduction of hydrogen into alpha quartz during sweeping," *Proc. 42nd. Ann. Freq. Contr. Symp.*, pp. 155–161, 1988.
[28] N. Oura, N. Kuramochi, M. Kushino, and T. Katsumoto, "Defects in synthetic quartz and the Q-values of the $-18.5°$ X-cut bar," *Jap. Jour. Appl. Phys.*, vol. 20, Suppl. 20–3, pp. 157–160, 1981.
[29] G. R. Johnson and R. A. Irvine, "Etch channels in single crystal quartz," *Proc. 41st. Ann. Freq. Contr. Symp.*, pp. 175–182, 1987.
[30] R. A. Laudise and R. L. Barns, "Perfection of quartz and its connection to crystal growth," *IEEE Trans. Ultrason. Ferroelect. Freq. Contr.*, vol. 35, no. 3, pp. 277–287, 1988.
[31] A. Zarka, L. Lin, and M. Buisson, "Influence de la localisation sectorielle du germe sur la qualite' cristalline," *J. Cryst. Growth*, vol. 54, pp. 394–398, 1981.
[32] A. F. Armington and J. J. Larkin, "Quartz growth on X-seeds," U.S. Patent 4 576 808, May 1986.
[33] A. R. Lang, "Studies of the individual dislocations in crystals by x-ray diffraction microradiography," *J. Appl. Phys.*, vol. 30, pp. 1748–1755, 1959.
[34] T. Hanyu, "Dislocation etch tunnels in quartz crystals," *J. Phys. Soc.*, Japan, vol. 19, p. 1489, 1964.
[35] A. R. Lang and V. F. Miuscov, "Dislocation and fault surfaces in synthetic quartz," *J. Appl. Phys.*, vol. 38, pp. 2477–2483, 1967.
[36] F. Iwasaki, "Line defects and etch tunnels in synthetic quartz," *J. Cryst. Growth*, vol. 39, pp. 292–298, 1977.
[37] J. W. Nielson and F. G. Foster, "Unusual etch pits in quartz crystals," *Amer. Min.*, vol. 45, pp. 299–310, 1960.
[38] N. Cabrera, M. M. Levine and J. S. Plaskett, "Hollow dislocations and etch pits," *Phys. Rev.*, vol. 96, p. 1153, 1954.
[39] W. Hanson, "Transmission X-ray topography of single crystal quartz using white beam synchrotron radiation," *Proc. 41st. Ann. Freq. Contr. Symp.*, pp. 228–235, 1987.
[40] C. Frondel, *The System of Mineralogy*, vol. III, Silica Minerals. New York and London: Wiley, 1962, esp. pp. 153–155.
[41] J. G. Gualtieri, "The influence of temperature and electric field on the etch-channel density in swept-cultured quartz," *Proc. 39th. Ann. Freq. Contr. Symp.*, pp. 247–254, 1985.
[42] ——, "Further studies on electrode-diffusion-suppressed-swept quartz," *Proc. 41st. Ann. Freq. Contr. Symp.*, pp. 192–198, 1987.
[43] J. Asahara, K. Nagai, K. Hamaguchi, H. Sone, and S. Taki, "An analytical study of electrodiffusion (sweeping) of synthetic quartz crystals," *Proc. 45th. Ann. Freq. Contr. Symp.*, pp. 9–21, May 1991.
[44] A. Ballato, "Doubly rotated thickness mode plate vibrators," in *Physical Acoustics: Principles and Methods*, W. P. Mason and R. N. Thurston, Eds. Orlando, FL: Academic, 1977, vol. 13, ch. 5, pp. 115–181.
[45] ——, "Piezoelectric resonators," in *Design of Crystal and Other Harmonic Oscillators*, by B. Parzen. New York: Wiley, 1985, pp. 66–122 and 432–436.
[46] G. K. Guttwein, T. J. Lukaszek, and A. Ballato, "Practical consequences of modal parameter control in crystal resonators," *Proc. 21st. Ann. Freq. Contr. Symp.*, pp. 115–137, Apr. 1967.
[47] R. A. Heising, *Quartz Crystals for Electric Circuits*. New York: Van Nostrand, 1946, ch. XII, esp. pp. 394–410.
[48] I. Avramov, "Extremely high-loop power GHz range surface transverse wave oscillators using AB-class amplifiers," *Proc. 1993 IEEE Freq. Contr. Symp.*, pp. 728–732, June 1993.
[49] A. Karaulnik and B. Grouzinenko, "Research aimed at designing a miniature ruggedized configuration of BVA-type crystal unit," *Proc. 1993 IEEE Freq. Contr. Symp.*, pp. 548–559, June 1993.
[50] I. Abramson, A. N. Dikidzhi, A. I. Kutalev, and S. V. Plachotin, "Application of TC-cut quartz resonators excited by lateral electrical field," *Proc. 1993 Freq. Contr. Symp.*, pp. 535–540, June 1993.
[51] J. A. Kosinski, A. Ballato, and Y. Lu, "Measured properties of doubly rotated dilithium tetraborate ($Li_2B_4O_7$) resonators and transducers," *IEEE Trans. Ultrason., Ferroelect., Freq. Contr.*, vol. 40, pp. 154–161, Mar. 1993.
[52] K. M. Lakin, G. R. Kline, R. S. Ketcham, A. R. Landin, W. A. Burkland, K. T. McCarron, S. D. Braymen, and S. G. Burns, "Thin film resonator technology," *41st. Ann. Freq. Contr. Symp.*, pp. 371–381, May 1987.
[53] K. M. Lakin, G. R. Kline, and K. T. McCarron, "High Q microwave acoustic resonators and filters," *Proc. 1993 IEEE MTT Symp.*, vol. 3, pp. 1517–1520; see also, "Overmoded high Q resonators for microwave oscillators," *1993 IEEE Int. Freq. Contr. Symp.*, pp. 718–721, June 1993.
[54] A. Ballato, J. Kosinski, and T. Lukaszek, "Lithium tetraborate transducers," *IEEE Trans. Ultrason., Ferroelect., Freq. Contr.*, vol. 38, pp. 62–66, 1991.
[55] G. K. Guttwein, A. Ballato, and T. J. Lukaszek, "VHF-UHF piezoelectric resonators," U.S. Patent 3 394 677, Sept. 1972.
[56] M. Berté, "Acoustic-bulk-wave resonators and filters operating in the fundamental mode at frequencies greater than 100 MHz," *Electron. Lett.*, vol. 13, pp. 248–250, 1977. Also published in *Proc. 31st. Ann. Freq. Contr. Symp.*, pp. 122–125, 1977.
[57] L. Bidart and J. Chauvin, "Direct frequency crystal oscillators," *Proc. 35th. Ann. Freq. Contr. Symp.*, pp. 365–375, May 1981.
[58] *Properties of Lithium Niobate*, London and New York: INSPEC, IEE, EMIS Datareviews Series No. 5, esp. pp. 32, 83, and 123.

Arthur Ballato (S'55–M'59–SM'71–F'81) for a biography, see p. 59 of the January 1994 issue of this TRANSACTIONS.

John G. Gualtieri (M'81–SM'91) for a biography, see p. 58 of the January 1994 issue of this TRANSACTIONS.